Angular correlation, spin alignment, and resonance behavior in $^{12}C+^{12}C$ inelastic scattering

A. H. Wuosmaa, D. J. Hofman,* B. B. Back, D. J. Blumenthal,† S. Fischer,‡ D. J. Henderson, R. V. F. Janssens, C. J. Lister, V. Nanal,§ D. Nisius,‖ M. D. Rhein¶ and P. R. Wilt
Physics Division, Argonne National Laboratory, Argonne, Illinois 60439
(Received 13 September 2001; published 16 January 2002)

We have studied α-^{12}C angular correlations for peaks observed in the $^{12}C[^{12}C,^{12}C(3_1^-)]^{12}C(0_1^+)$ inelastic-scattering excitation function in the energy range between $E_{c.m.}=25$ to 35 MeV. The excitation-function data for α-particle angles that correspond to the population of specific magnetic substates in the excited, decaying ^{12}C nucleus suggest that these peaks are associated with a preferentially aligned configuration. The angular-correlation data are consistent with spin assignments of $J^\pi=16^+$ and 18^+ for the resonancelike structures observed at $E_{c.m.}=27.5$ MeV and 33.1 MeV, respectively. The observed alignment, and the deduced spin values are consistent with a dinuclear configuration for these peaks.

DOI: 10.1103/PhysRevC.65.024609 PACS number(s): 25.70.Ef, 25.70.Pq

I. INTRODUCTION

The observation of resonances in elastic and inelastic scattering reactions between light, heavy ions has intrigued nuclear physicists for the better part of four decades. The system in which this phenomenon figures most prominently is $^{12}C+^{12}C$ [1], where a variety of features have been reported over a wide range of bombarding energies, in the elastic channel, as well as in many inelastic and other reaction channels. Generally, two paradigms have been employed to describe this behavior. In one picture, the resonances arise as a consequence of the nuclear structure at high excitation energy in ^{24}Mg, as suggested by calculations carried out using the cranked-shell model [2], cranked-cluster model [3] or Hartree Fock [4] formalism. An alternative description lies in the idea that peaks in the elastic or inelastic scattering cross sections represent scattering phenomena, i.e., they correspond to scattering resonances in the ion-ion potential, or even more simply to kinematic windows with favorable momentum and angular-momentum matching properties. A number of reaction-model formalisms have been qualitatively successful in describing many features of these inelastic scattering reactions (e.g., [5–8]). In light of recent experimental developments, these methods have been refined and some new predictions have become available [9–11]. The common idea that has persisted for many years is that the resonances in the scattering of two ^{12}C nuclei correspond to a very extended, dinuclear molecular configuration, where the properties of the scattering system may reflect a sensitivity to reaction dynamics, as well as to the nuclear structure of the colliding ions and of the composite system. With the renewed interest in nuclear properties at the extreme conditions of angular momentum and excitation energy that has accompanied the study of ''superdeformed'' states in heavier nuclei, and with the availability of sophisticated new detector systems, a revisitation of these issues is appropriate.

Despite considerable experimental and theoretical effort over the years, progress in the understanding of many of these phenomena has been slow. One problem is that, while the energy dependence of the scattering cross section in many reaction channels has been well studied, the detailed spectroscopic data necessary to test theories are still lacking. As an example, consider the situation encountered in the $^{12}C+^{12}C$ system for the bombarding energy region between 20 and 40 MeV in the center-of-mass system. Here, several prominent, intermediate-width structures were observed by Cormier *et al.* in single, and mutual inelastic scattering to the first excited 2_1^+ (4.443 MeV) state [12,13], and by Fulton *et al.* in inelastic scattering to the 3_1^-(9.64 MeV) $+0_1^+$(0.0 MeV) and 0_2^+(7.65 MeV)$+0_1^+$, final states [14]. The features in these different channels appear at approximately similar, but not identical beam energies. Also, the nuclear structures of the states in ^{12}C for these inelastic scattering channels are somewhat different. It remains uncertain whether the observed cross section peaks are in some way related to each other, or simply appear at common bombarding energies due to the complicated overall spectrum of resonancelike structures in virtually all $^{12}C+^{12}C$ inelastic scattering channels. A correspondence between peaks in the excitation curves for different scattering channels is especially difficult to establish in the absence of detailed spectroscopic information, such as firm spin assignments.

For reaction channels with nonzero spin, such spectroscopic data are in general difficult to obtain. For the resonances in the $2_1^+ + 0_1^+$ and $2_1^+ + 2_1^+$ channels, initial spin assignments were suggested based upon a comparison to data for light-charged-particle reactions in the same energy range [12,15]. Later, using a technique based upon a line-shape analysis for $^{12}C(2_1^+)+^{12}C(0_1^+)$ inelastic scattering, Sugiyama *et al.* concluded that the prior spin ''suggestions''

*Present address: Physics Department, University of Illinois at Chicago, Chicago, IL 60607-7059.
†Present address: Bechtel Nevada, P.O. Box 38, Suitland, MD 20752.
‡Present address: DePaul University, Chicago, IL 60614.
§Present address: Department of Nuclear and Atomic Physics, Tata Institute of Fundamental Research, Homi Bhaba Road, Colaba, Mumbai 400 005, India.
‖Present address: BIR Inc., Lincolnshire, IL 60069.
¶Present address: Gesellschaft für Schwerionenforschung, Planckstrassse 1, D-64291 Darmstadt, Germany.

were probably in error by two units of angular momentum [16,17]. Particle–γ-ray angular-correlation methods also proved useful in understanding resonance behavior in this [18] and other heavy-ion scattering systems [19–22], and in some cases unambiguous resonance spin assignments could be obtained.

Such angular-correlation measurements have also proved useful in the evaluation of reaction mechanisms, via the study of spin alignment. Trombik *et al.* [23] and Konnerth *et al.* [24] performed detailed particle-γ, and particle-γ-γ angular-correlation measurements in the $^{12}C+^{12}C$ system for single, and mutual 2_1^+ inelastic scattering, respectively. They demonstrated that the configuration in which the spins of the excited ^{12}C nuclei are aligned with the orbital angular momentum plays a significant role in the scattering process, as expected in the simple picture of a dinuclear, molecular complex.

For states that decay by particle, rather than γ-ray, emission, similar measurements can be done. If the emitted particle is an α particle, with zero intrinsic spin, the interpretation of the angular-correlation data may, in principle, also be used to obtain spin assignments for resonances in inelastic scattering reactions involving nonzero channel spin [25–28]. One example is in inelastic scattering to the $^{12}C(3_1^-)$ state at 9.64 MeV, where Fulton *et al.* have reported resonancelike features. Reactions populating the $^{12}C(3_1^-)$ state are interesting from the point of view of nuclear structure, as well as reaction mechanisms. The 3_1^- state in ^{12}C state has been attributed to an equilateral-triangular arrangement of α particles similar to that of the ground state, but with a larger separation between the α-cluster centers [29–32]. With a large channel excitation energy, but modest channel spin, the $3_1^-+0_1^+$ channel is not as well matched in angular momentum as channels involving the 2_1^+ state, but these kinematic factors could be compensated by an increased moment of inertia introduced by the larger effective radius of the 3_1^- state. Also, channel coupling effects for the 3_1^- state might be expected to be between those involving the compact ground state, or 2_1^+ excitations, and extended, cluster configurations such as the excited 0_2^+ state.

Previously, we have presented results from one such study for a peak observed by Fulton *et al.* in the $^{12}C(3_1^-)+^{12}C(0_1^+)$ excitation function near $E_{\mathrm{c.m.}}=33$ MeV [27]. In that measurement, the sequential α decay of the 3_1^- state to the ground state of ^{8}Be $[^{12}C(3_1^-)\rightarrow\alpha+^8\mathrm{Be}(2\alpha)]$ was observed using silicon strip detectors at five bombarding energies across the peak in the excitation function, and the measured angular correlations were used to assign a spin to the resonance. In the current work, we present a more detailed study of this reaction, performed over a wider bombarding energy range, and using a more powerful experimental setup that provides significantly enhanced efficiency and acceptance than that used previously. These results extend our understanding of the properties of this inelastic scattering channel and support the interpretation of cross section peaks as ''dinuclear'' resonances characterized by unique angular-momentum quantum numbers.

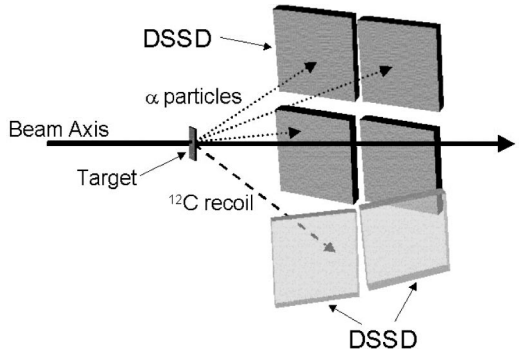

FIG. 1. Schematic diagram of the experimental setup. The dotted lines denote the directions of α particles from the decay of the excited ^{12}C nucleus, and the dashed line the direction of the recoiling ^{12}C.

II. EXPERIMENT

The techniques for studying charged-particle angular correlations used in this work have been described previously [27,33]. Briefly, to study the $^{12}C(^{12}C,^{12}C[3_1^-])^{12}C[0_1^+]$ reaction, the α particles from the decaying $^{12}C(3_1^-)$ state were detected in a large solid-angle array of four double-sided silicon strip detectors (DSSDs), each 5 cm $\times$5 cm in area, placed on one side of the beam. The two faces of each DSSD were divided into sets of 16 strips. The two sets were orthogonal to each other, and yielded an arrangement of 256 ''quasipixels.'' Each quasipixel had an angular acceptance of approximately 1° in the laboratory. The typical energy resolution of each strip was between 50 and 100 keV for 8 MeV α particles. The detectors making up this array were placed at distances between 16 and 19 cm from the target. The complete array subtended a total laboratory solid angle of approximately 330 msr. Data were taken with the four DSSD array centered at two angles $\theta_{lab}=25°$ and 35° to increase the sensitive angle range. Two additional DSSDs, located on the opposite side of the beam, were used only to check the beam energy as described below. Also, two monitor detectors were used to measure the beam flux and target thickness through small angle elastic scattering. A schematic diagram of the experimental setup appears in Fig. 1.

The experiment was carried out with ^{12}C beams produced by the ATLAS accelerator at Argonne National Laboratory. Beams with intensities of approximately 10–15 pnA, at 13 energies between $E_{lab}=50$ to 69 MeV, bombarded ^{12}C foils with an areal density of 50 μg/cm^2. The beam was bunched in buckets of width $\approx$500 ps, 82 ns apart, and the time of flight of the particles relative to the accelerator rf signal was used for particle identification. The beam current was integrated in a Faraday cup to provide a cross-check on the absolute normalization obtained from the monitor detectors. All experimental parameters, including the energy, flight time, and position of each detected particle, were recorded on tape. The total dead time of the acquisition system was measured using a pulser, and was typically no more than 20–30 %. The absolute value of the beam energy was checked by recording events in which both ^{12}C nuclei were dissociated into three α particles, and all six of these were detected. In that case,

the total energy deposited in the strip detectors was equal to the beam energy minus the six α-particle breakup energy of approximately 15 MeV. Although limited by statistics, this measurement was able to determine the beam energy to a precision of approximately 500 keV in the laboratory, and was in good agreement with the value obtained from the accelerator beam-energy measurement system [34].

The efficiency for the coincident detection of three α particles in the four DSSD array is a complicated function of bombarding energy, scattering and α-particle emission angle, and was determined using a Monte Carlo simulation. For each beam energy, we generated 2×10^6 $^{12}C(3_1^-)+^{12}C(0_1^+)$ events in which the decaying ^{12}C nucleus was emitted into the solid angle subtended by the four DSSD array. The excited ^{12}C nucleus was then made to decay sequentially into $\alpha+^8Be_{g.s.}(2\alpha)$. The detector efficiency was determined by counting the number of simulated events in which all three α particles struck the four DSSD array. Effects such as multiple α particles hitting single strips, and the presence of nonworking strips, were included in the simulations. In all cases the inelastic $^{12}C+^{12}C$ scattering angular distribution was assumed to be isotropic, as was the angular distribution of the α-$^8Be_{g.s.}$ decay. The sensitivity of the total detection efficiency to these angular distributions was in general small in the center of the acceptance.

Some results of these calculations are summarized in Fig. 2. Figure 2(a) displays the bombarding energy dependence of the three-α detection efficiency, integrated over all angles, expressed in terms of the effective solid angle seen by the scattered $^{12}C(3_1^-)$ nuclei. The total efficiency of the four DSSD array varied from approximately 10% to 12% for the 25° detector setting over the range of bombarding energies covered. For the 35° setting, the efficiency was reduced due to the smaller average recoil velocities of the decaying ^{12}C nuclei, and ranged from 6% to 9% for $E_{lab}=52$ to 70 MeV. Figure 2(b) illustrates the scattering-angle dependence of the efficiency at a bombarding energy of $E_{lab}=65.15$ MeV, for the two angle settings of the four DSSD array. The efficiency is roughly constant for a range of $\Delta\theta_{c.m.}\approx40°$ in the center of the acceptance.

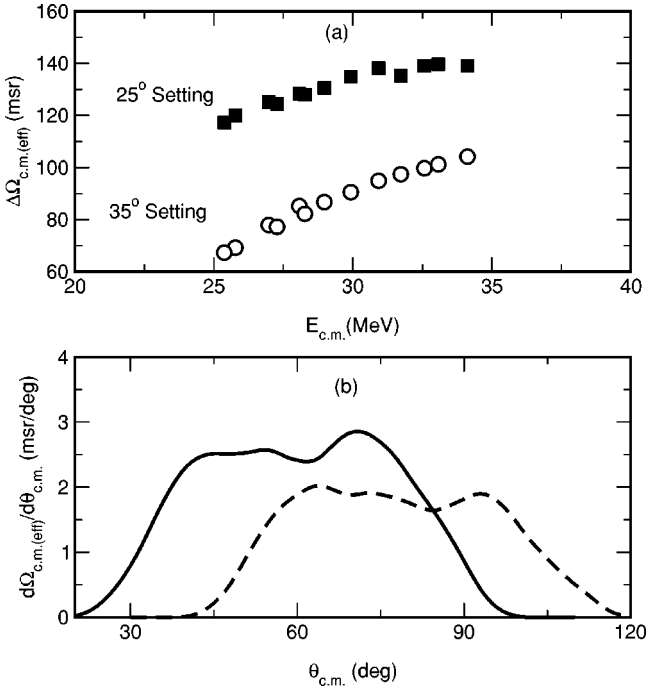

FIG. 2. (a) Bombarding energy dependence of the three-α detection efficiency for the $3_1^-+0_1^+$ excitation, expressed as the effective solid angle in the center-of-mass system. The filled squares, and open circles symbols correspond to the values for the 25° and 35° settings of the four DSSD array, respectively. (b) Scattering angle dependence for the three-α detection efficiency for the $3_1^-+0_1^+$ excitation at $E_{lab}=65.15$ MeV. The solid and dashed lines correspond to the 25° and 35° settings of the four DSSD array, respectively.

III. DATA REDUCTION AND ANALYSIS

The method for reducing the raw experimental data—α-particle energies and angles—into the quantities needed to extract the angular-correlation results have been described in previous publications [27,33] and will only be reviewed briefly here. The energies and the angles of the three detected α particles are used to compute their momentum vectors. This information, combined with the beam energy, is sufficient to reconstruct the excitation energy of the decaying ^{12}C, to identify which two of the three α particles came from the decaying $^8Be_{g.s.}$ fragment, and to calculate the $^{12}C+^{12}C$ scattering angle and Q value. Typical results are summarized in Fig. 3. Figures 3(a) and 3(b) display the excitation energy spectra reconstructed for α-α pairs and 3α combinations, respectively, assuming that they are produced by the decay of $^8Be_{g.s.}$ and ^{12}C. For the ^{12}C excitation-energy spectrum in Fig. 3(b), only events in which the excited ^{12}C nucleus is observed to decay into $\alpha+^8Be_{g.s.}$ are included. This requirement reduces background contributions from other reaction channels or from scattering.

After deducing the ^{12}C excitation energy from Fig. 3(b), the kinetic energy and scattering angle were reconstructed from the α-particle momenta, and these were used to calculate the reaction Q value, as shown in Fig. 3(c). Here, only events for which the decaying ^{12}C nucleus is in the 3_1^- state are histogrammed. The most prominent feature in the spectrum corresponds to the channel of interest, the $3_1^-+0_1^+$ peak at $Q=-9.64$ MeV. All subsequent analysis focuses on the events associated with this peak.

A. Angular distributions

To extract the $3_1^-+0_1^+$ angular distribution, the data for this excitation were sorted according to the scattering angle, and then corrected for the angle-dependent three-α detection efficiency described above. The absolute normalization for each energy was obtained from forward-angle elastic-scattering data measured with the small solid-angle monitor detectors. These data were compared with the results of optical-model calculations carried out using the potential parameters of Reilly *et al.* [35]. The total inelastic-scattering cross section was determined at each energy by integrating the measured angular distribution.

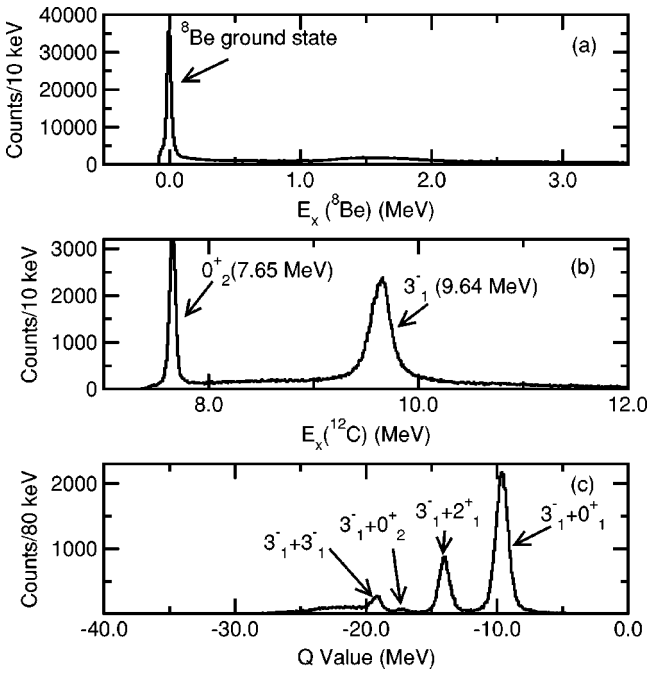

FIG. 3. (a) Reconstructed ^{8}Be$_{g.s.}$ excitation-energy spectrum from α-particle pairs detected in the four-DSSD array. (b) Reconstructed ^{12}C excitation-energy spectrum from three α particles detected in the four DSSD array, for events with $E_X(^8\mathrm{Be}_{g.s.})=0$ MeV. (c) Reconstructed ^{12}C+^{12}C Q-value spectrum for events with $E_X(^8\mathrm{Be}_{g.s.})=0.0$ MeV and $E_X(^{12}\mathrm{C})=9.64$ MeV.

B. Angular correlations

An important facet of the present work is the extraction of the angular correlation, or the double-differential cross section $\mathrm{d}^2\sigma/\mathrm{d}\Omega_\theta \mathrm{d}\,\Omega_\psi$. The angle θ corresponds to the scattering angle in the $^{12}\mathrm{C}(3^-_1)+^{12}\mathrm{C}(0^+_1)$ center-of-mass system $\theta_{\mathrm{c.m.}}$, while ψ represents the angle of the relative $\alpha-^8\mathrm{Be}_{g.s.}$ velocity in the center-of-mass frame of the decaying ^{12}C nucleus, measured relative to the beam axis, as described in Refs. [25–27]. The data were sorted into $\theta_{\mathrm{c.m.}}-\psi$ matrices as described in Ref. [27]. The three-α detection efficiency was obtained from Monte Carlo simulations as a function of $\theta_{\mathrm{c.m.}}$ and ψ, and was used to transform the raw data into the appropriate angular correlations. The dependence of this efficiency on $\theta_{\mathrm{c.m.}}$ and ψ is similar to that described in Ref. [27].

IV. RESULTS

A. Excitation functions

The measured energy dependence of the yield for the $3^-_1+0^+_1$ channel is illustrated in Fig. 4(a), which presents the scattering cross section integrated between the center-of-mass scattering angles 40° to 105° (open circles), and compared with the cross sections reported by Fulton *et al.* [14] from $\theta_{lab}=15°$ to 25° (filled squares), corresponding to center-of-mass angles between 35° and 57° at $E_{lab}=50$ MeV, to between 32° and 54° at $E_{lab}=68$ MeV. The present data show enhancements near $E_{\mathrm{c.m.}}=28$ and, more notably, 33 MeV. The 33 MeV peak is prominent in the Fulton *et al.* data, however, the double-peak structure reported in Ref. [14] between 25 and 29 MeV is not fully reproduced. Instead, a single, smaller peak is observed here at 28 MeV. In the prior work, these structures were compared with the predictions of the band crossing model (BCM) [6–8], with the suggestion that the dominant angular momenta at $E_{\mathrm{c.m.}}\approx 26$, and 32 MeV were $14\hbar$ and $16\hbar$, respectively. The complexity of the spectrum, however, suggested that the simple BCM was not able to reproduce all the features of the data.

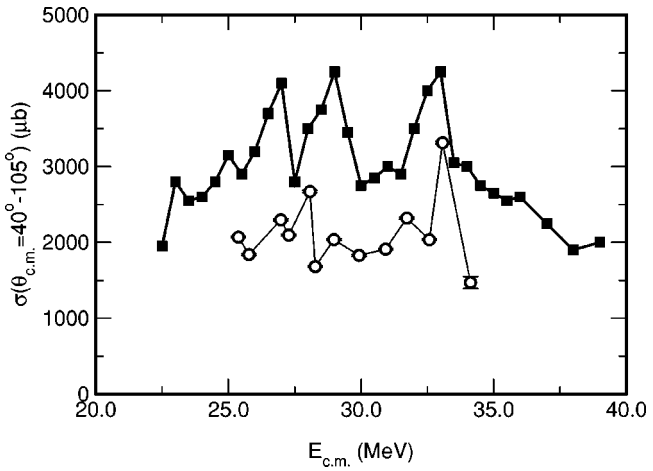

FIG. 4. $^{12}\mathrm{C}(3^-_1)+^{12}\mathrm{C}(0^+_1)$ excitation-function data. The open symbols show the data from the present experiment, integrated from $\theta_{\mathrm{c.m.}}=40°-105°$. The data from Fulton. *et al.* [14] for $\theta_{lab}=15°-25°$ are the filled squares.

It has been shown in other reactions that the energy dependence of the cross section for particular magnetic substates can provide considerable additional information about the scattering process [16,20,21]. In principle, such information may be obtained by studying the energy dependence of the α-^{12}C angular correlations. In the present case, however, the lack of complete cylindrical symmetry and a complicated acceptance preclude a reliable extraction of the cross section associated with each magnetic substate. Some of this information can be obtained, however, by examining the data at particular values of the α-particle emission angle ψ. For example, if the decay α particle is detected at $\psi=0°$ or 180°, then regardless of the ^{12}C scattering angle θ, the data reflect the behavior of the $m=0$ magnetic substate in the coordinate system with the quantization axis chosen to lie along the beam direction. Other choices of ψ have similar significance. At $\psi=90°$, only odd magnetic substates can contribute to the angular correlation and therefore, the data reflect the behavior of $\sigma_{m=1}$ and $\sigma_{m=3}$. If the system is strongly aligned, then the cross section from the $m=3$ substate is small, and the yield here is dominated by the $m=1$ magnetic substate. Similarly, at $\psi\approx 63°$ or 117°, the associated Legendre Polynomial $P^m_3(\psi)$ is approximately zero for $m=1$. For a strongly aligned configuration, the $m=3$ contribution is again small, and the yield is now dominated by $m=0$ and 2.

Figures 5(a)–(c) show the energy dependence of the cross section integrated from $\theta_{\mathrm{c.m.}}=40°$ to 105°, for $\Delta\psi=10°$ wide intervals centered at $\psi=5°$ and 175°, $\approx 63°$ and 117°, and 90°, respectively. The cross section integrated over the

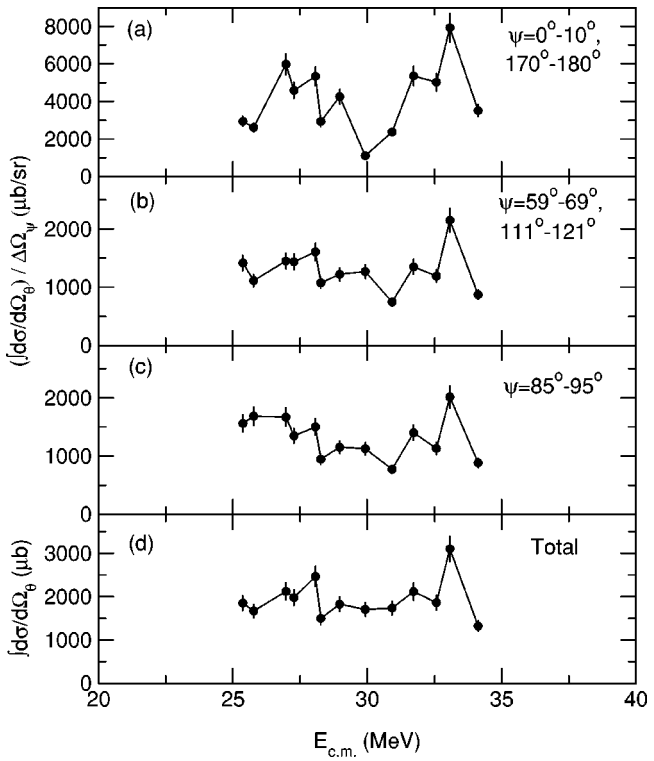

FIG. 5. $^{12}C(3_1^-)+^{12}C(0_1^+)$ excitation-function data integrated from $\theta_{c.m.}=40°-95°$ for (a) $\psi\approx 0°$,180°, (b) $\psi\approx 63°$,117°, and (c) $\psi\approx 90°$. (d) Total integrated cross section for $\theta_{c.m.}=40°-105°$.

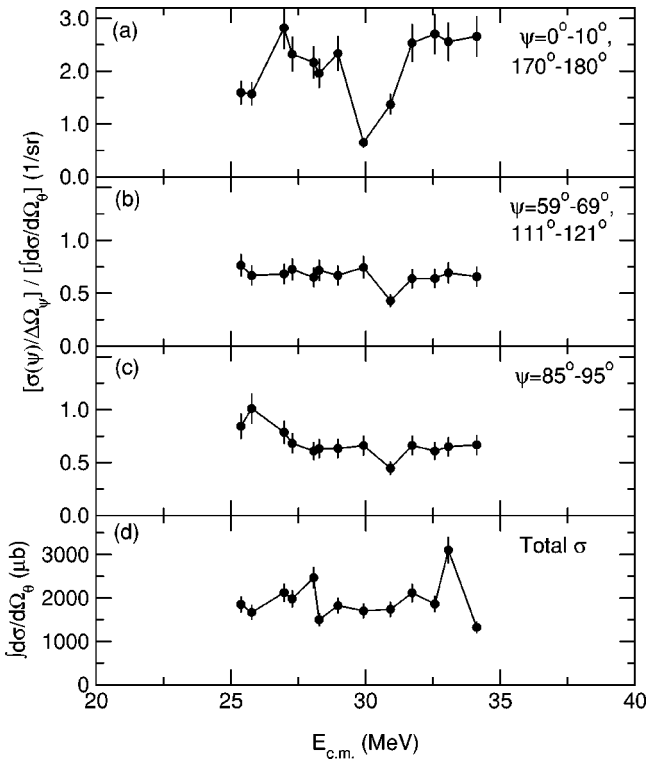

FIG. 6. Ratio of angle-averaged cross section for $^{12}C(3_1^-)+^{12}C(0_1^+)$ inelastic scattering at $\psi\approx 0°$,180° (a) $\psi=63°$,117° (b), and $\psi\approx 90°$ to the cross section ($\psi=0°-180°$). (d) Total integrated cross section.

angular range covered in the present experiment is given for comparison in Fig. 5(d). The largest yield is observed for $\psi\approx 0°$ and 180°, suggesting an enhancement in the $m=0$ substate population relative to other values of *m*, as expected for an aligned configuration. The enhancements observed in the integrated cross section also appear in the ψ-angle selected data, with the peak-to-''background'' ratio largest for data obtained with $\psi=0°$ and 180°.

The magnetic-substate population parameters P_m are given by the ratio between the cross section for individual magnetic substates σ_m and the total cross section. Although the present data are insufficient to extract all of the σ_m, the behavior related to that of the individual magnetic-substate population parameters can be obtained by studying the cross section obtained at different ψ angles divided by the integrated cross section, as illustrated in Fig. 6. The ratio for $\psi=0°$ and 180°, directly related to the $m=0$ magnetic-substate population parameter, shows the strongest enhancement at the energies near those corresponding to the resonances previously identified by Fulton *et al.*, whereas the ratios for the other values of ψ are approximately constant with bombarding energy. This result suggests that the orientation of the spin of the excited $^{12}C(3_1^-)$ fragment is preferentially perpendicular to the beam direction, as was previously observed in the particle–γ-ray angular-correlation measurements of Trombik *et al.* [23] and Konnerth *et al.* [24] for other $^{12}C+^{12}C$ inelastic scattering channels, and indicate that the observed peaks may not be simple cross section fluctuations, but rather could reflect interesting reaction phenomena.

B. Angular distributions

For elastic or inelastic scattering to a spin-zero final state, the conventional method used to determine spin assignments involves performing a partial-wave decomposition of the angular distributions. For final states with nonzero spin, this method is no longer suitable as the oscillations in the angular distributions for different magnetic substates are out of phase with one another, yielding a total angular distribution that is largely featureless. For single inelastic scattering through an isolated resonance with spin *J* decaying with a single partial wave *L* in the exit channel with channel spin *S*, the angular distribution is given by

$$\sigma(\theta_{c.m.})=\sum_m |\langle LS-mm|J0\rangle P_L^m(\theta_{c.m.})|^2, \qquad (1)$$

where the relative amplitudes of the associated Legendre polynomials P_L^m are given by the Clebsch-Gordan coefficients, and *m* ranges from $-S$ to *S*. For the aligned choice $L=J-S$, this angular distribution is completely featureless.

Figures 7 and 8 show the angular-distribution data obtained at each beam energy for the $^{12}C(0_1^+)+^{12}C(3_1^-)$ channel. The falloff of the data at the most forward and backward angles, and the resulting apparent asymmetry about 90°, likely reflect an imperfect calculation of the experimental

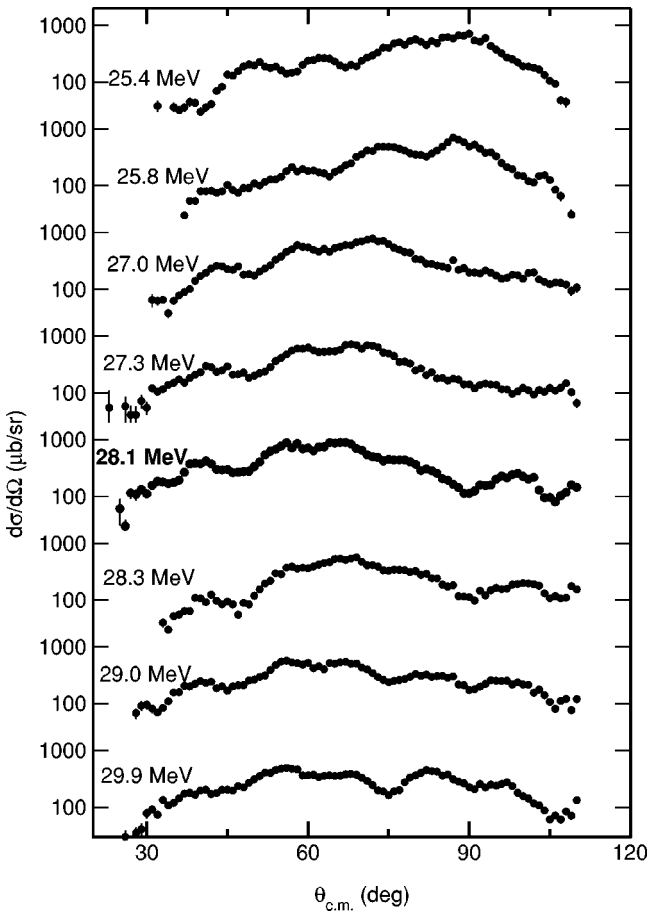

FIG. 7. $^{12}C(3_1^-)+^{12}C(0_1^+)$ angular distributions for $E_{c.m.}=25.4$ MeV to 29.9 MeV.

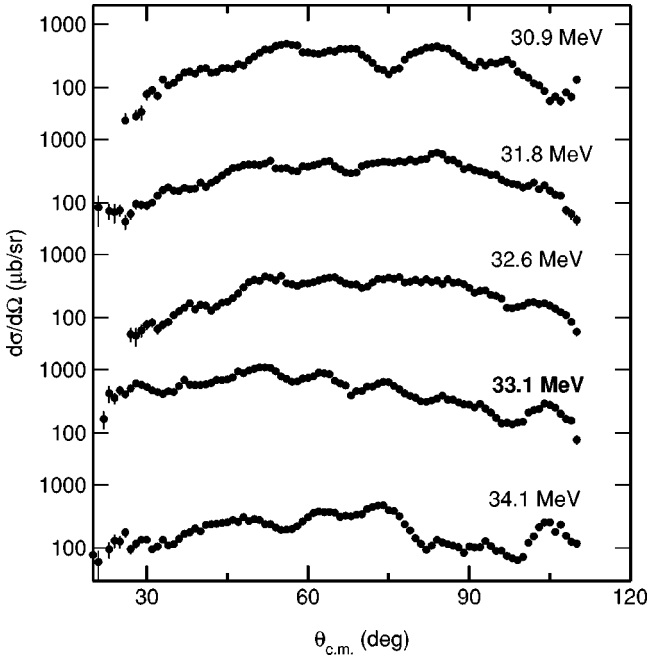

FIG. 8. $^{12}C(3_1^-)+^{12}C(0_1^+)$ angular distributions for $E_{c.m.}=30.9$ MeV to 34.1 MeV.

efficiency at the edges of the experimental acceptance. The data exhibit some oscillatory features, likely reflecting the fact that several partial waves are present in the exit channel, and that the very simple assumption implicit in Eq. (1) for a fully aligned configuration is not entirely fulfilled. These features, however, give no obvious clues to the values of the dominant orbital angular momenta. Clearly without further analysis, these data are of little use in determining the values of the spins of resonances in this energy region.

C. Angular correlations

1. $\psi=0°$, 180°

In order to address more fully the questions of contributing angular momenta, we decompose the cross section into components characterized by the correlated decay α particle and the $^{12}C+^{12}C$ scattering angles, ψ and θ. As discussed above, measurements at a particular angle ψ permit a nearly model-independent analysis of the data. The most obvious choice is $\psi=0°$ or 180°, where only the $m=0$ substate can contribute. In a partial-wave decomposition of the $m=0$ cross section, the angular distribution $\sigma(\theta_{c.m.})|_{\psi=0°,180°} \equiv \sigma_0(\theta_{c.m.})$ can be expressed simply as a coherent sum of Legendre polynomials,

$$\sigma_0(\theta_{c.m.})=\left|\sum_L a_L P_L(\cos\theta_{c.m.})\right|^2. \qquad (2)$$

Figures 9 and 10 present scattering angular distributions for the $3_1^-+0_1^+$ channel at the various beam energies studied, where the α particle from the $^{12}C(3_1^-)\rightarrow\alpha+^8Be_{g.s.}$ decay is observed near $\psi=0°$ or 180°. In contrast to the data shown in Figs. 7 and 8, the $\psi=0°$,180° angular distributions are strongly oscillatory. In particular, at the energies corresponding to the peaks in the excitation function, the oscillations are remarkably regular. The maxima and minima in the angular distributions at these energies are nearly in phase with those in the curves calculated from pure squared Legendre polynomials of degree 13 and 15 near $E_{c.m.}=27.5$, and 33.1 MeV, respectively, as illustrated by the dashed curves in Figs. 9 and 10. This comparison suggests that these partial waves are the dominant ones in the outgoing channel at these energies.

We have performed partial-wave fits to these data, using an expression of the form of Eq. (2), where the complex parameters a_L represent the different partial-wave amplitudes. Two sets of fits were carried out, using three, and then four partial waves, $L=(11,13,15)$, and $L=(11,13,15,17)$, respectively. A variety of starting conditions were used for each set of fits. The introduction of additional partial waves with L less than 11 or greater than 17 did not significantly improve the quality of the fits. The fit results were chained together, so that the final results of the fit at one energy formed the starting point for the chi-square minimization procedure at the next energy. The results were found to be stable with respect to variations in starting parameters. The results appear as the solid curves in Figs. 9 and 10. The thin dot-dashed, and thick curves represent the fit results with three, and four partial waves, respectively. The quality of the fits is fair, with the best results obtained at the maxima of the

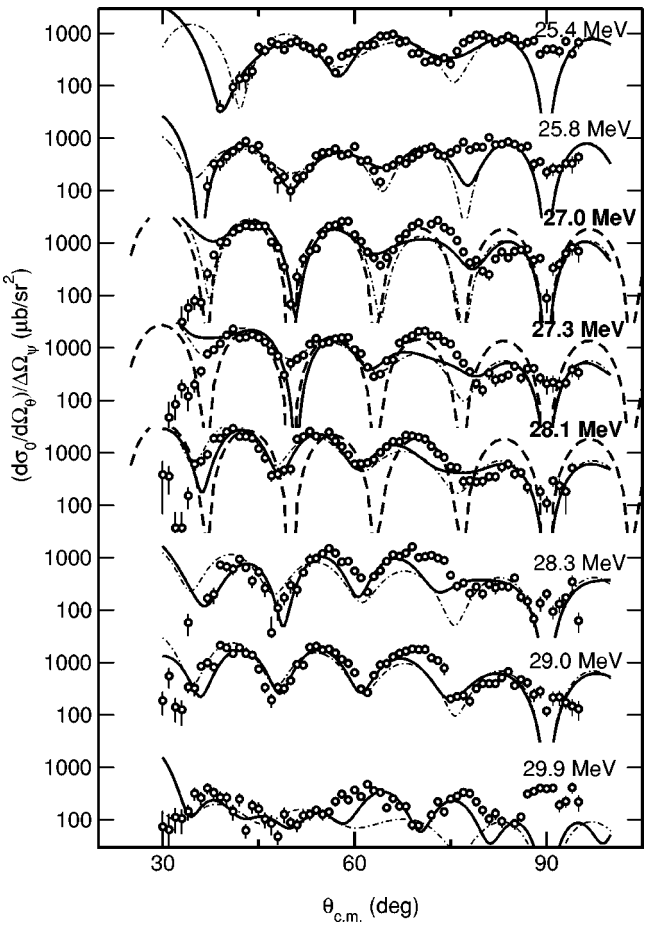

FIG. 9. $^{12}C(3_1^-)+^{12}C(0_1^+)$ angular distributions for $E_{c.m.}=25.4$ MeV to 29.9 MeV, for $\psi\approx 0°,180°$. The solid curves correspond to partial-wave Legendre-polynomial fits with $L=11$–15 (thin dot-dashed curves) and $L=11$–17 (thick curves). The dashed curves for $E_{c.m.}=27.0$, 27.3, and 28.1 MeV represents $|P_{13}(\cos\theta)|^2$.

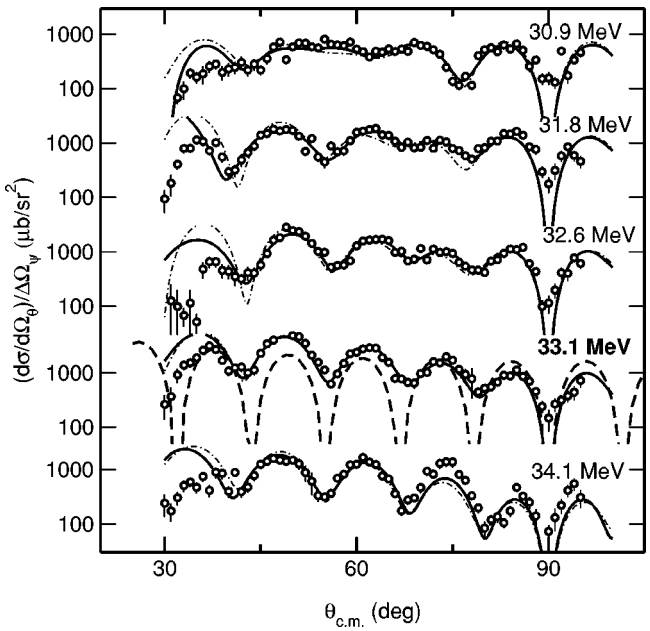

FIG. 10. $^{12}C(3_1^-)+^{12}C(0_1^+)$ angular distributions for $E_{c.m.}=30.9$ MeV to 34.1 MeV, for $\psi\approx 0°,180°$. The solid curves correspond to partial-wave Legendre-polynomial fits with $L=11$–15 (thin dot-dashed curves) and $L=11$–17 (thick curves). The dashed curve for $E_{c.m.}=33.1$, MeV represents $|P_{15}(\cos\theta)|^2$.

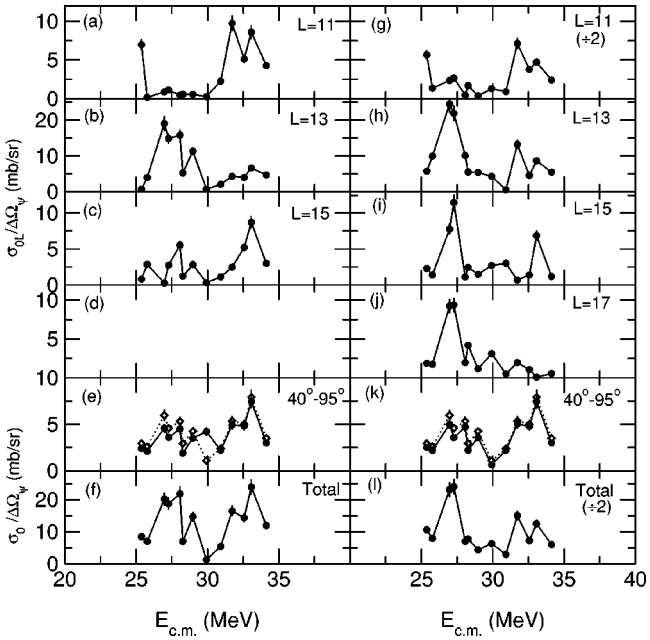

FIG. 11. Results of partial-wave fits to the $m=0$ angular-distribution data. (a)–(c) Partial cross section $\sigma_L=4\pi|a_L|^2/(2L+1)$ from the fits with $L=11$–15. (e) Three partial-wave fit result integrated from $\theta_{c.m.}=40°$ to 95° (solid symbols) and data (open symbols). (f) $\sigma_{0tot}=\Sigma_L\sigma_{0L}$ from the three partial-wave fit. (g)–(j) Partial cross section $\sigma_L=4\pi|a_L|^2/(2L+1)$ from the fits with $L=11$–17. (k) Four partial-wave fit result integrated from $\theta_{c.m.}=40°$ to 95° (solid symbols) and data (open symbols). (l) $\sigma_{0tot}=\Sigma_L\sigma_{0L}$ from the four partial-wave fit.

excitation function where, if the peak does actually represent a resonance in the reaction, a single partial wave should make a significant contribution to the cross section. At most energies, the addition of $L=17$ does not change the quality of the fit appreciably; one exception is at $E_{c.m.}=29.9$ MeV, where neither fit can reproduce the maximum near 90°, which must reflect complex interference phenomena, or an $m\neq 0$ contribution introduced by the fact that the measurement is not carried out strictly at $\psi=0°$.

The energy dependence of the extracted $m=0$ partial-wave cross sections $\sigma_{0L}=4\pi|a_L|^2/(2L+1)$ appears in Figs. 11(a)–(c) for $L=11,13$, and 15, and Figs. 11(g)–(j) for $L=11,13,15$, and 17. Figures 11(e) and 11(k) show the corresponding results obtained from the fits integrated over the angle range covered in the experiment, 40° to 95°, with the measured points shown for comparison as open diamonds. Finally, Figs. 11(f) and 11(l) display the total $m=0$ cross section $\sigma_{0tot}=\Sigma_L 4\pi|a_L|^2/(2L+1)$. The results of the fits with three partial waves confirm our previous expectations from simple inspection of the $m=0$ angular distributions, namely, that $L=13$ is the most important partial wave for the

lower energy peak, and $\sigma_{0,L=15}$ shows a narrow enhancement at $E_{\mathrm{c.m.}}=33$ MeV. The comparison between the data and the fit results for the angle-integrated cross section in Fig. 11(e) is reasonably good except for at $E_{\mathrm{c.m.}}=29.9$ MeV, where the three-L fit clearly under predicts the data in Fig. 9. The situation with the four partial-wave fits is more complicated. Whereas the only significant improvement in the fit quality gained from the addition of $L=17$ is at $E_{\mathrm{c.m.}}=29.9$ MeV, as seen in Fig. 11(l), the energy dependence of the $m=0$ partial-wave cross sections, as well as the $m=0$ total cross section, has changed dramatically compared to the three partial-wave fit. Specifically, a strong peak is seen for $L=13$, 15, and 17, near $E_{\mathrm{c.m.}}=27$ MeV, that does not appear in the $m=0$ angle-integrated cross section in Fig. 11(k). This observation suggests that the total cross section results from these latter fits are dominated by contributions at forward angles where the fits are not constrained by data, and may not be reliable. Still, for $E_{\mathrm{c.m.}}=33$ MeV, the $L=15$ component is the only one that displays a narrow peak consistent with that observed in the total $3_1^-+0_1^+$ excitation curve shown in Fig. 4.

The partial-wave analysis is consistent with the current partial-wave assignments of $L=13$ and 15 for the two peak energies, however, due to the differences between the two sets of fits, as well as the quality of the fits, it is desirable to try to find a less ambiguous procedure. One method advocated by Balamuth *et al.* [36] and Chapuran *et al.* [37], is to study the energy dependence of the cross section at angles corresponding to zeros of different Legendre polynomials. In such an analysis, a resonance in a particular partial wave should appear as a peak in the zero-angle excitation curves for every value of L *except* for the one that resonates. We have analyzed our $\psi=0°$,180° angular-correlation data in this manner. The results are shown in Fig. 12, which represents the zero functions $Z_L=\Sigma_i\sigma_0(\theta_{Li})$, where the θ_{Li} are the angles at which the Legendre polynomial of order L is zero, and the cross section is summed over a 1° wide interval around each θ_{Li}. For the lower energy peak at $E_{\mathrm{c.m.}}=27.5$ MeV, the peak is observed clearly in Z_L for $L=11$,15, and 17, but is completely absent for $L=13$, supporting the $L=13$ assignment at this energy. For the higher energy peak, some structure is observed in each of the four Z functions, although the data for $L=15$ show the weakest such behavior. This result, combined with the energy dependence of the partial-wave amplitudes, and the simple comparison of the data to single squared Legendre polynomials, all support a firm $L=15$ assignment for the structure at $E_{\mathrm{c.m.}}=33.1$ MeV.

2. $\psi=63°$, 117°

This picture is reinforced by angular-correlation data obtained at decay-α-particle angles of $\psi=63°$ and 117°. Here, we define $\sigma(\theta_{\mathrm{c.m.}})|_{\psi=63,117}\equiv\sigma_{m\neq1}$, as these angles correspond to zeros of $P_3^1(\psi)$, and thus there is no $m=1$ substate contribution to the cross section. The character of the θ dependence of the yield can then provide some information on the degree of alignment of the system. At the θ angles covered in the present experiment, the associated Legendre polynomials $P_L^0(\theta)$ and $P_L^2(\theta)$ are approximately in phase, and $P_L^3(\theta)$ is out of phase with the P_L^ms with even m. For an isolated resonance with spin J decaying through a single L value, as seen from Eq. (1), the contributions from the different magnetic substates are given by the squares of the values of the Clebsch-Gordan coefficients $|\langle LS-mm|J0\rangle|^2$. The relevant Clebsch-Gordan coefficients for the aligned $(L=J-S)$, and one nonaligned case $(L=J-S+2)$ are listed in Table I. For the aligned case, the $m=3$ contribution is negligible, and the angular correlation at ψ angles corresponding to zeros of $P_L^1(\psi)$ should be oscillatory. If the system is not strongly aligned, the introduction of an $m=3$ component can result in weaker oscillations, or a possible maximum at $\theta_{\mathrm{c.m.}}=90°$, in the angular distribution for these values of ψ.

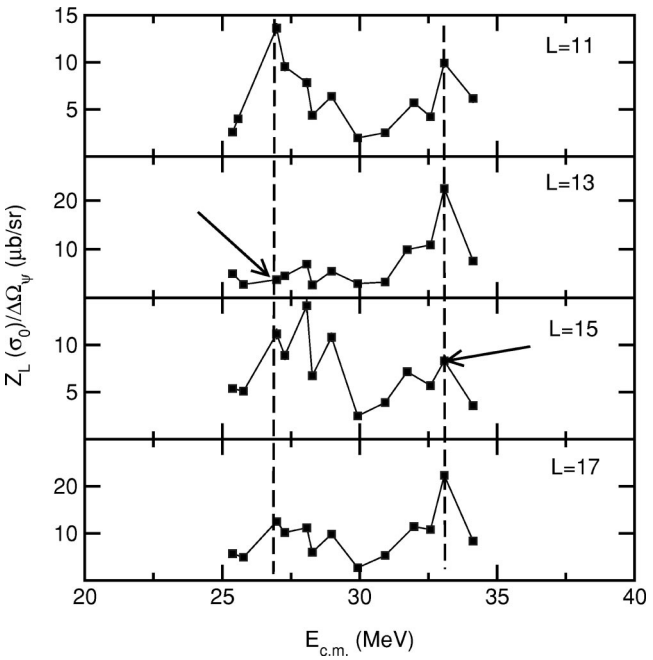

FIG. 12. Energy dependence of the $m=0$ cross section at the zeros of different Legendre polynomials, $Z_L(\sigma_0,E_{\mathrm{c.m.}})$. The arrows indicate the positions of total cross section maxima.

Figures 13 and 14 show the scattering angular distributions for the $3_1^-+0_1^+$ channel, at the different beam energies

TABLE I. Clebsch-Gordan coefficients relevant to $3_1^-+0_1^+$ inelastic scattering, for a $J=18$ resonance, decaying either to the aligned $(L=J-3=15)$ or nonaligned $(L=J-3+2=17)$ cases.

J	L	S	m	$(2-\delta_{m,0})\lvert\langle LS-mm\rvert J0\rangle\rvert^2$
18	15	3	0	0.342
18	15	3	1	0.480
18	15	3	2	0.320
18	15	3	3	0.020
18	17	3	0	0.194
18	17	3	1	0.015
18	17	3	2	0.390
18	17	3	3	0.400

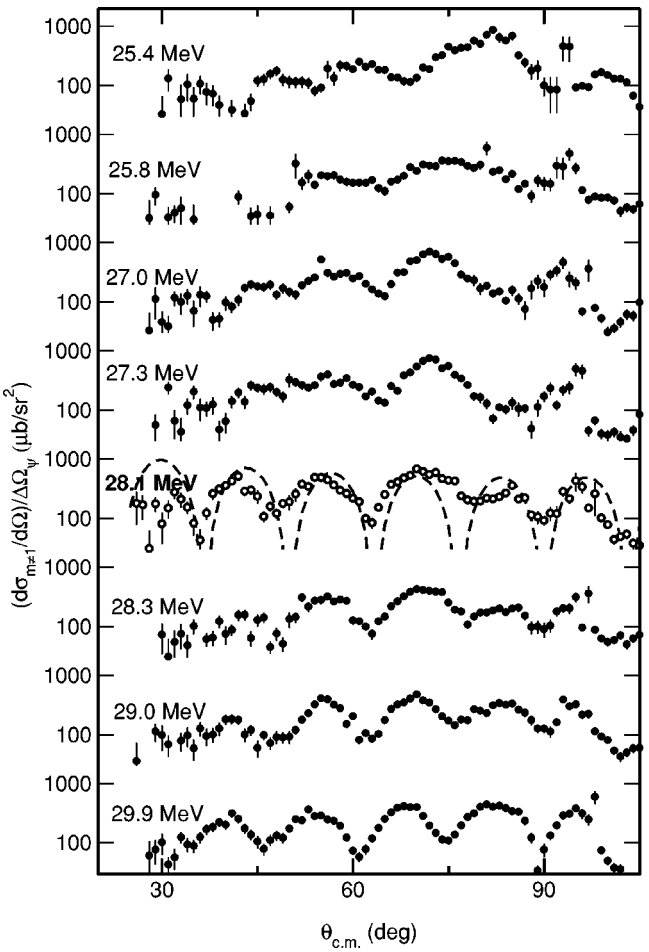

FIG. 13. Angular distributions for $E_{\text{c.m.}}=25.4$ MeV to 29.9 MeV, for $\psi=63°,117°$. The dashed curve for $E_{\text{c.m.}}=28.1$ MeV represents $|P_{13}(\cos\theta_{\text{c.m.}})|^2$.

studied, where the decay α particle is detected near either $\psi=63°$ or 117°. These angular distributions are not as strongly oscillatory as those obtained with $\psi=(0°,180°)$, although they show considerably more structure than what is seen in the total angular distributions. The data at the excitation-function peaks are in phase with pure squared Legendre polynomials of degree 13, and 15, as was observed for the data taken at $\psi=0°,180°$. For example, the dashed curves in Figs. 13 and 14 represent $|P_{13}(\cos\theta)|^2$ and $|P_{15}(\cos\theta)|^2$, for $E_{\text{c.m.}}=28.1$ and 33.1 MeV, respectively, and are in reasonable agreement with the data. This result, as well as the observation that there exists no discernible maximum in these angular distributions near $\theta_{\text{c.m.}}=90°$, supports the the assumption that the system is preferentially aligned at the energies at which the cross section shows resonancelike behavior, as well as the L-value assignments obtained from the $\psi=0°,180°$ data. With the demonstration of an aligned configuration with $J=L+S$, we may extend our L-value determinations to spin assignments of $J^\pi=16^+$ at $E_{\text{c.m.}}=27.5$ MeV, and $J^\pi=18^+$ at $E_{\text{c.m.}}=33.1$ MeV. For the peak at $E_{\text{c.m.}}=33.1$ MeV, these results are in agreement with our previous measurements [27].

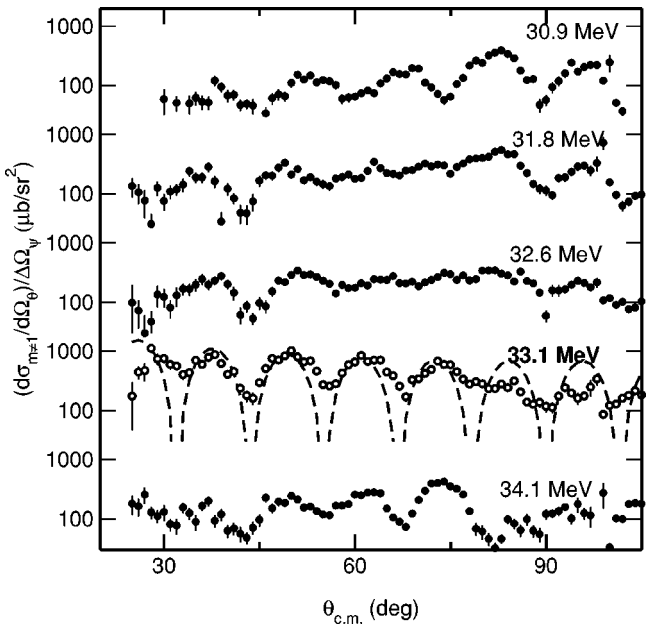

FIG. 14. Angular distributions for $E_{\text{c.m.}}=30.1$ MeV to 29.9 MeV, for $\psi=63°,117°$. The dashed curve for $E_{\text{c.m.}}=33.1$ MeV represents $|P_{15}(\cos\theta_{\text{c.m.}})|^2$.

V. DISCUSSION

It is interesting to examine the present results in light of earlier speculations about inelastic scattering in this energy region, as well as in the context of structure model, and reaction-model descriptions of resonances in $^{12}\text{C}+^{12}\text{C}$ scattering. The angular momenta suggested by the present data appear to be inconsistent with the spin ''suggestions'' made for resonances in the 2_1^+ and $2_1^+ + 2_1^+$ channels at approximately the same energies, where Cormier *et al.* [12] proposed spins of $14\hbar$ and $16\hbar$ at energies of $E_{\text{c.m.}}=25$, and 31 MeV, respectively. This conclusion could mean either that the resonances in the $3_1^- + 0_1^+$ channel are unrelated to those in the light-particle evaporation channels upon which the earlier spin suggestions were based, or that the prior spin suggestions are incorrect, or both. The magnetic-substate angular-distribution measurements of Sugiyama *et al.* tend to support spin assignments for resonances in the $2_1^+ + 0_1^+$ channel that are closer to those obtained in the present work. If the structures observed in the $3_1^- + 0_1^+$ channel are linked to those present in other channels, it is likely that the spins of those resonances are two units of angular momentum higher than previously suggested.

The results of the present measurements may also be compared to simple pictures of the $^{12}\text{C}+^{12}\text{C}$ system. For instance, assuming centroid energies of $E_{16}=27.5\pm0.5$ MeV, and $E_{18}=33.1\pm0.25$MeV for the 16^+, and 18^+ states, respectively, and assuming further that these two resonances are part of a rotational sequence with $E_J=E_0+(\hbar^2/2I)\times J(J+1)$, we deduce a moment-of-inertia parameter $\hbar^2/2I=80\pm10$ keV. This value is very close to that obtained from a simple calculation assuming two touching spheres each with $R_{12_C}=1.2A^{1/3}=2.74$ fm ($\hbar^2/2I=79$ keV), although it is somewhat smaller than that ob-

tained from the cranked-cluster model calculations of the $^{12}C+^{12}C$ band in ^{24}Mg (configuration "F1" in Ref. [3], with $\hbar^2/2I=90$ keV). Kamimura tabulates the calculated rms mass radii of various states in ^{12}C [32], and gives $R(0_1^+)=2.40$ fm, and $R(3_1^-)=2.76$ fm. These radii lead to a value of $\hbar^2/2I=100$ keV for a hypothetical ground-state band—very close to the value of $\hbar^2/2I=105$ keV derived from the sequence of states in the $2_1^+ + 0_1^+$ channel if one adjusts the spins in Ref. [12] upward by two units. A rotational sequence from two touching spheres, one with $R(0_1^+)$ and one with $R(3_1^-)$, has $\hbar^2/2I=88$ keV, closer to that from the present data. Although the uncertainties on the moment-of-inertia parameters from the present data, and from the Cormier *et al.* assignments, are large due to the uncertainty in the centroid energies for the different resonances, there appears to be a difference in the moment of inertia between the resonances in the two reaction channels. Additional measurements for the $3_1^- + 0_1^+$ channel could bear out this suggestion.

Finally, it is also useful to place the current results into the context of past, and recent, reaction-model calculations for $^{12}C+^{12}C$ scattering. The early BCM calculations [6–8] for the $3_1^- + 0_1^+$ channel placed the centroids of the 14^+, and 16^+ strength at $E_{\mathrm{c.m.}} \approx 26$ MeV and 32 MeV, respectively. These calculations were in general agreement with the earlier spin assignments for the $2_1^+ + 0_1^+$ and $2_1^+ + 2_1^+$ excitations. The current results suggest that these calculations are, as with the prior spin assignments, two units of angular momentum too low. One earlier problem with the results of the BCM for the $3_1^- + 0_1^+$ excitation was that the experimental spectrum was more complicated, and the states narrower, than given by the BCM. Our data suggest that the spectrum may actually be simpler than previously thought, and that at least the $J^\pi = 16^+$ resonance may be somewhat wider than the individual members of the previously reported doublet, in better agreement with the simple BCM predictions.

A comparison of our results for the $3_1^- + 0_1^+$ channel with new calculations is complicated by the fact that the most recent coupled-channels results of Hirabayashi *et al.* [9] and Ito *et al.* [10,11] do not report any predictions for the behavior of this particular excitation. The method of Hirabayashi and Ito attempts to treat the $^{12}C+^{12}C$ scattering problem by considering both shell-model like states ("shell group" or SG) and with 3-α particle cluster character ("cluster group" or CG) in ^{12}C in a coupled-channels formalism. In contrast to the earlier BCM calculations, the ion-ion potential is derived from a double-folding prescription, and also includes the effects of quadrupole distortions in the mass distributions of the excited states. This modification substantially alters the band-crossing properties of the different reaction channels. Without the effects of channel coupling, the calculation predicts a series of potential resonances with the 16^+ and 18^+ states lying near the structures observed in the current data. The widths of the potential resonances, with $\Gamma_{\mathrm{c.m.}} \approx 1-2$ MeV, are also comparable to those of the observed features. The effects of channel coupling fragment the strength for each partial wave, producing narrow features dominated by wave-function components in the various participating channels. Little evidence is seen in the present data for such narrow ($\Gamma_{\mathrm{c.m.}} < 100$ keV) features, although the center-of-mass energy resolution for the current data set might preclude the observation of such narrow structure.

As discussed earlier, the structure and excitation energy of the $^{12}C(3_1^-)$ state suggest that inelastic scattering reactions involving it will behave somewhere between those exclusively involving the ground and first excited 2_1^+ levels, and the clustered 0_2^+ states. Reference [11] predicts that the dominant contributions to $J^\pi = 16^+$ and 18^+ strength between $E_{\mathrm{c.m.}} = 25$ MeV and 35 MeV are predominantly from resonances in the $[2_1^+ \otimes 0_1^+]_{I=2,L=J-2}$, $[2_1^+ \otimes 2_1^+]_{I=4,L=J-4}$, $[2_1^+ \otimes 2_1^+]_{I=2,L=J-2}$, $[2_1^+ \otimes 0_1^+]_{I=2,L=J}$, and $[2_1^+ \otimes 2_1^+]_{I=4,L=J-2}$ SG subchannels, where in the notation of Ref. [11] I is the channel spin, J is the resonance spin, and L the decay angular momentum. These subchannels are for the most part either partially, or fully aligned in angular momentum. The angular-momentum matching properties of the $3_1^- + 0_1^+$ excitation may be expected to lie between those of the $[2^+ \otimes 2^+]_{I=4,L=J-4}$ and $[2^+ \otimes 2^+]_{I=4,L=J-2}$ subchannels, while the nuclear structure of the 3_1^- state suggests a rotational band with a slightly larger moment of inertia than those for the "SG" channels in Ref. [11]. These speculations would place our current results for the $3_1^- + 0_1^+$ channel in approximate agreement with the results of Ref. [11], however, a calculation that explicitly includes this channel, and makes detailed predictions for its behavior would be very useful.

VI. CONCLUSION

We have performed detailed particle-particle angular-correlation measurements for resonances observed in $^{12}C(3_1^-)+^{12}C(0_1^+)$ inelastic scattering. The present data support spin assignments of $J^\pi = 16^+$ and 18^+ for resonances at $E_{\mathrm{c.m.}} = 27.5$ MeV and 33.1 MeV, respectively. These resonances decay with dominant L values of $L=13$ and 15, and a predominantly aligned configuration ($L = J - S$), consistent with the expectations for a dinuclear molecular system. These data provide additional constraints for theoretical attempts to describe resonance behavior in the inelastic scattering of $^{12}C+^{12}C$, and add to the rather small body of available spectroscopic data for resonances in channels with nonzero channel spin.

ACKNOWLEDGMENTS

This work was supported by the U.S. Department of Energy, Nuclear Physics Division under Contract No. W-31-109-Eng38. A.H.W. wishes to thank R. H. Siemssen for helpful comments and discussions.

[1] R. R. Betts and A. H. Wuosmaa, Rep. Prog. Phys. **60**, 819 (1997), and references therein.
[2] G. Leander and S. E. Larsson, Nucl. Phys. **A239**, 93 (1975).
[3] S. Marsh and W. D. M. Rae, Phys. Lett. B **180**, 185 (1986).
[4] J. Cugnon, H. Dombre, and H. Flocard, Nucl. Phys. **A331**, 213 (1979).
[5] B. Imanishi, Nucl. Phys. **A125**, 33 (1969).
[6] T. Matsuse, Y. Kondō, and Y. Abe, Prog. Theor. Phys. **59**, 1009 (1978).
[7] Y. Kondō, Y. Abe, and T. Matsuse, Phys. Rev. C **19**, 1356 (1979).
[8] Y. Abe, T. Matsuse, and Y. Kondō, Phys. Rev. C **19**, 1365 (1979).
[9] Y. Hirabayashi, Y. Sakuragi, and Y. Abe, Phys. Rev. Lett. **74**, 4141 (1995).
[10] M. Ito, Y. Sakuragi, and Y. Hirabayashi, Eur. Phys. J. A **5**, 373 (1999).
[11] M. Ito, Y. Sakuragi, and Y. Hirabayashi, Phys. Rev. C **63**, 064303 (2001).
[12] T. M. Cormier, J. Applegate, G. M. Berkowitz, P. Braun-Munzinger, P. M. Cormier, J. W. Harris, C. M. Jachcinski, L. L. Lee, Jr., J. Barrette, and H. E. Wegner, Phys. Rev. Lett. **38**, 940 (1977).
[13] T. M. Cormier, C. M. Jachckinski, G. M. Berkowitz, P. Braun-Munzinger, P. M. Cormier, M. Gai, J. W. Harris, J. Barrette, and H. Wegner, Phys. Rev. Lett. **40**, 924 (1978).
[14] B. R. Fulton, T. M. Cormier, and B. J. Hermann, Phys. Rev. C **21**, 198 (1980).
[15] H. Feshbach, J. Phys. (Paris) Colloq. **37**, C5 177 (1976).
[16] Y. Sugiyama, Y. Tomita, H. Ikezoe, and N. Shikazono, Z. Phys. A **322**, 579 (1985).
[17] Y. Sugiyama, N. Shikazono, Y. Tomita, H. Ikezoe, T. Takekoshi, E. Takekosi, S. Kubono, and M. Tanaka, Phys. Lett. **159B**, 90 (1985).
[18] L. E. Cannell, R. W. Zurmühle, and D. P. Balamuth, Phys. Rev. Lett. **43**, 837 (1979).
[19] C. M. Jachinski, P. Braun-Munzinger, G. M. Berkowitz, R. H. Friefelder, M. Gai, R. C. McGrath, R. Paul, T. Renner, and C. D. Ulhorn, Phys. Lett. **87B**, 354 (1979).
[20] A. H. Wuosmaa, R. W. Zurmühle, P. H. Kutt, S. F. Pate, S. Saini, M. L. Halbert, and D. C. Hensely, Phys. Rev. Lett. **58**, 1312 (1987).
[21] A. H. Wuosmaa, R. W. Zurmühle, P. H. Kutt, S. F. Pate, S. Saini, M. L. Halbert, and D. C. Hensely, Phys. Rev. C **41**, 2666 (1990).
[22] S. F. Pate, R. W. Zurmühle, A. H. Wuosmaa, P. H. Kutt, M. L. Halbert, D. C. Hensley, and S. Saini, Phys. Rev. C **41**, R1344 (1990).
[23] W. Trombik, W. Trautmann, F. Krug, W. Dünnweber, D. Konnerth, W. Hering, R. Singh, and D. Zeppenfeld, Phys. Lett. **135B**, 271 (1984).
[24] D. Konnerth, W. Dünnweber, W. Hering, W. Trautmann, W. Trombik, W. Zipper, D. Habs, W. Hennerici, H. J. Hennrich, R. Kroth, A. Lazzarini, R. Repnow, V. Metag, and R. S. Simon, Phys. Rev. Lett. **55**, 588 (1985).
[25] W. D. M. Rae and R. K. Bhowmik, Nucl. Phys. **A427**, 142 (1984).
[26] R. K. Bhowmik, W. D. M. Rae, and B. R. Fulton, Phys. Lett. **136B**, 149 (1984).
[27] A. H. Wuosmaa, B. B. Back, R. R. Betts, M. Freer, B. G. Glagola, D. J. Henderson, D. J. Hofman, and V. Nanal, Phys. Rev. C **54**, 2463 (1996).
[28] S. P. G. Chappell, D. L. Watson, S. P. Fox, C. D. Jones, W. D. M. Rae, P. M. Simmons, M. Freer, B. R. Fulton, N. M. Clarke, N. Curtis, M. J. Leddy, J. S. Pople, S. J. Hall, R. P. Ward, G. Tungate, W. N. Catford, C. Y. Gyapong, S. M. Singer, and P. H. Regan, Phys. Rev. C **51**, 695 (1995).
[29] N. Takigawa and A. Arima, Nucl. Phys. **A168**, 593 (1970).
[30] E. Uegaki, S. Okabe, Y. Abe, and H. Tanaka, Prog. Theor. Phys. **57**, 1262 (1977).
[31] E. Uegaki, Y. Abe, S. Okabe, and H. Tanaka, Prog. Theor. Phys. **62**, 1621 (1979).
[32] M. Kamimura, Nucl. Phys. **A351**, 456 (1981).
[33] A. H. Wuosmaa, P. Wilt, B. B. Back, R. R. Betts, M. Freer, B. G. Glagola, Th. Happ, D. H. Henderson, I. G. Bearden, R. W. Zurmühle, D. P. Balamuth, S. Barrow, D. Benton, Q. Li, Z. Liu, and Y. Miao, Nucl. Instrum. Methods Phys. Res. A **345**, 482 (1994).
[34] R. C. Pardo, B. E. Clifft, P. Denhartog, D. Kovar, W. Kutschera, and K. E. Rehm, Nucl. Instrum. Methods Phys. Res. A **270**, 226 (1988).
[35] W. Reilly, R. Wieland, A. Gobbi, M. W. Sachs, J. Maher, R. H. Siemssen, D. Mingay, and D. A. Bromley, Nuovo Cimento A **13**, 913 (1973).
[36] D. P. Balamuth, T. Chapuran, C. M. Laymon, W. K. Wells, and D. P. Bybell, Phys. Rev. Lett. **55**, 2842 (1985).
[37] T. Chapuran, D. P. Balamuth, W. K. Wells, C. M. Laymon, and D. P. Bybell, Phys. Rev. C **34**, 2358 (1986).